Terahertz photoresponse of AlInSb/InSb/AlInSb quantum well structures

F. Gouider,[1] Yu. B. Vasilyev,[2] M. Bugár,[3] J. Könemann,[4] P. D. Buckle,[5] and G. Nachtwei[1]
[1]*Institut für Angewandte Physik, Technische Universität Braunschweig, D-38106 Braunschweig, Germany*
[2]*Ioffe Physical Technical Institute, Russian Academy of Science (RAS), 194021 St. Petersburg, Russia*
[3]*Institute of Physics, Charles University–Prague, CZ-12116 Prague 2, Czech Republic*
[4]*Physikalisch-Technische Bundesanstalt, D-38116 Braunschweig, Germany*
[5]*QinetiQ Ltd., Malvern WR14 3PS, United Kingdom*
(Received 12 January 2010; revised manuscript received 8 March 2010; published 2 April 2010)

We have studied the photoresponse (transmission and photoconductivity of Corbino-shaped devices) of structures with InSb quantum wells (AlInSb barriers). To characterize the devices, the Shubnikov-de Haas (SdH) effect up to magnetic fields B of 7 T and current-voltage (I-V) characteristics at various magnetic fields were measured. Some of the samples showed clearly resolvable SdH oscillations. The I-V curves showed pronounced nonlinearities. The phototransmission and the photoconductivity at various terahertz (THz) frequencies were measured around 2.5 THz generated by a p-Ge laser. From the cyclotron resonance (transmission measurements) we deduced a cyclotron mass of $0.022m_0$. We also performed photoconductivity measurements on Corbino-shaped devices in the THz frequency range. Oscillations of the photoconductivity with maxima near the minima of the conductivity in the dark were observed. Thus, these devices are potentially suitable for the detection of THz radiation.

DOI: 10.1103/PhysRevB.81.155304 PACS number(s): 78.67.De, 71.70.Di, 72.20.Ht

I. INTRODUCTION

The terahertz (THz) spectral range is very interesting for both fundamental physics and for applications such as active explosive detection, medical imaging of dry samples, and high bandwidth communication networks. However, it is rather complicated to generate and to transmit and detect electromagnetic waves of wavelengths around 150 μm (frequencies around 2 THz). These waves occur in the spectral range of far infrared radiation which is typical for blackbody emitters held at temperatures of about 30 K. It is difficult to generate the corresponding high frequencies electronically. Moreover, the optical generation of wavelengths longer than 100 μm is problematic. It is difficult to transfer waves of $\lambda \approx 150$ μm into atmospheric air. This is because atmospheric air contains water (H_2O) and carbon dioxide (CO_2). These molecules possess energy levels due to bond rotation which are spaced energetically such that waves of $\lambda \approx 150$ μm are strongly absorbed. The detection of THz waves is also rather complicated, in particular, if simultaneously a high sensitivity and a spectral selectivity of the detecting system are required. For the generation of THz waves we use a p-Ge laser system.[1,2] Our laser is continuously tunable in the wavelength range $120 \leq \lambda \leq 180$ μm,[3] by the magnetic field on the Ge crystal.

The monochromatic THz radiation is transferred to our samples via a 0.32 m long brass waveguide immersed in liquid helium. The sample under investigation is placed at the end of the waveguide and in the center of a second superconducting coil which can generate magnetic fields (B) up to 12 T (see Refs. 3 and 4). We use quantum-Hall (QH) detectors[3] of various materials[3,4] for the detection of the THz radiation. These QH detectors are simultaneously fast (response times less than 10 ns are achievable) and spectrally sensitive.[3] In this study we present observations of the photoresponse (PR) obtained at samples made from wafers with InSb quantum wells (QWs) embedded in barriers of AlInSb. We observed the cyclotron resonance (CR) of electrons in these wafers by the measurement of the transmission of THz waves through the sample as a function of the magnetic field B applied perpendicular to the wafer (Faraday configuration). Further, we measured the photoconductivity (PC) in Corbino-shaped devices made from the AlInSb/InSb/AlInSb wafers. To perform these measurements at appropriate values of B and of the source-drain voltage V_{SD} applied to these devices we measured the Shubnikov-de Haas (SdH) effect and (at certain B values) the current-voltage characteristics (I_{SD}-V_{SD} curves) in advance.

II. EXPERIMENTAL DETAILS

In this study we present magnetotransport and magneto-optical data obtained in the magnetic field range $0 < B < 7$ T at QH detectors patterned as Corbino rings on $Al_xIn_{1-x}Sb/InSb/Al_xIn_{1-x}Sb$ quantum-well wafers using a Ge detector. The transmission measurements were made on unpatterned squares of about 4×4 mm^2 pieces of the wafers. The $InSb/Al_xIn_{1-x}Sb$ heterostructures were grown by solid source molecular-beam epitaxy onto GaAs substrates. In growth order the structure consists of an accommodation layer to lattice match to a 3 μm $Al_{0.10}In_{0.90}Sb$ buffer, a 30 nm InSb QW and a 70 nm $Al_{0.15}In_{0.85}Sb$ top cap. Tellurium (Te) delta doping is incorporated into the top cap at a distance of 25 nm from the top of the QW.

From the magnetotransport data (SdH effect, see Fig. 1) we obtained an electron density of $n_s = 2.8 \times 10^{15}$ m^{-2} and an electron mobility of $\mu = 4.2$ m^2 V^{-1} s^{-1}.

At various magnetic fields corresponding to SdH minima we also measured current-voltage (I-V) characteristics of our Corbino samples. At a magnetic field of $B = 6$ T we observed a pronounced nonlinearity in the I-V curve in one of our samples (see inset of Fig. 1). Therefore, the sample investi-

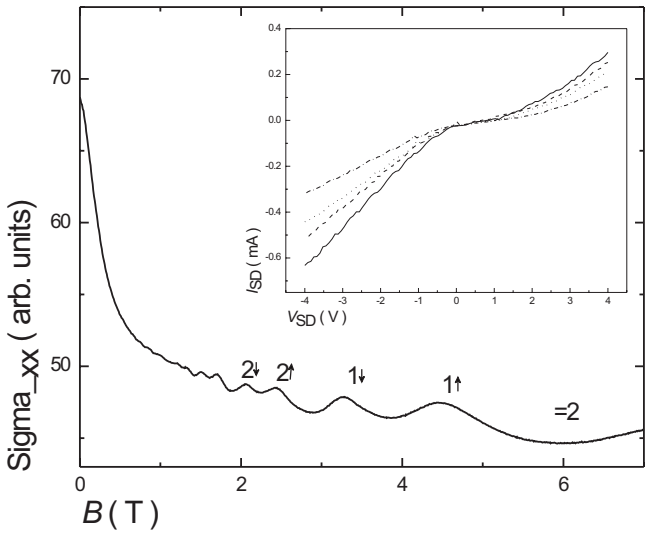

FIG. 1. Magnetoconductivity $\sigma_{xx}(B)$ for magnetic fields up to 7 T for a AlInSb/InSb/AlInSb quantum well sample. SdH oscillations are visible for $B>1$ T. The quantum numbers and the spin orientations corresponding to the SdH maxima are shown. The inset shows I_{SD}-V_{SD} curves measured at various SdH minima [at $B=1.85$ T (solid line), $B=2.86$ T (dashed line), $B=3.88$ T (dotted line), and $B=6.0$ T (dash-dotted line)].

gated appeared suitable as a QH detector for THz waves. With this sample, we studied the photoconductivity as a function of B at various frequencies around 2.5 THz [corresponding to a photon energy interval of $9.46 \leq E_{ph} \leq 10.30$ meV, see Fig. 3(a)]. The Ohmic contacts of the samples were annealed at two different temperatures of $T_{anneal}=420$ and of 520 K. For both types of samples photoconductivity signals were observable. However, for samples prepared using $T_{anneal}=520$ K, far higher values of the photoconductivity were measured for corresponding devices patterned in the Corbino geometry. An annealing temperature of $T_{anneal}=420$ K was applied first to avoid thermally induced decompositions of the devices. We found far better contact properties for $T_{anneal}=520$ K and no decomposition effects in the devices prepared using the higher annealing temperature.

III. EXPERIMENTAL INVESTIGATIONS

In Fig. 1 we show a SdH curve ($0<B<7$ T) for the AlInSb/InSb/AlInSb quantum well sample prepared using an annealing temperature of $T_{anneal}=420$ K. The inset shows I-V curves (I_{SD} versus V_{SD}) measured at different magnetic fields corresponding to minimum values of the conductivity σ_{xx} of the SdH curve. All these I_{SD}-V_{SD} curves are nonlinear. The most pronounced nonlinearity was observed at $B=6.0$ T corresponding to a filling factor of $\nu=2$. The decrease in σ_{xx} with increasing magnetic field is typical for samples having a Corbino shape.

For samples with Ohmic contacts prepared with an annealing temperature of $T_{anneal}=520$ K a larger signal of the photoconductivity signal was observable. To determine the value of the cyclotron mass m_c, we performed transmission

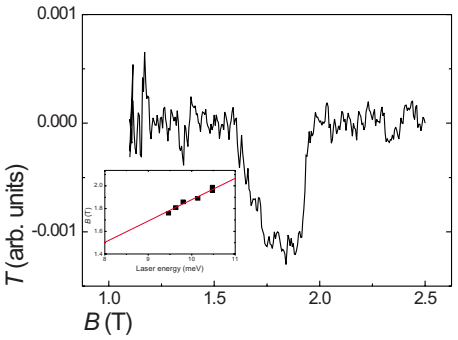

FIG. 2. (Color online) Transmission signal measured at a 4×4 mm^2 square of the wafer at $B=1.85$ T ($\nu=6$) at a photon energy $E_{ph}=9.68$ meV of the p-Ge laser. The inset shows the magnetic field position of the resonance minimum as a function of the laser energy in the range of $9.46 \leq E_{ph} \leq 10.48$ meV. This dependence is linear yielding a cyclotron mass of $m_c=(0.0218\pm0.0003)m_0$ (see the text). The magnetic field B is applied perpendicular to the wafer (corresponding to the Faraday configuration).

measurements using the radiation of the p-Ge laser with different photon energies in the range $9.46 \leq E_{ph} \leq 10.30$ meV (see inset of Fig. 2). For a photon energy of $E_{ph}=9.68$ meV (see Fig. 2) the transmission signal (measured with a Ge detector) as a function of the magnetic field B applied perpendicular to the wafer (Faraday configuration) is presented. The minimum value of the transmission was observed at $B=1.85$ T, corresponding to a cyclotron mass of $m_c=0.0218m_0$. A reference measurement was done using the same Ge detector but with no sample present. From the energy dependence of the CR minimum we deduced $m_c=(0.0218\pm0.0003)m_0$. In Fig. 3(a) the PC measured within magnetic field range $1.2<B<3.0$ T is displayed in relation to the SdH curve $\sigma_{xx}(B)$ for various photon energies of $9.46 \leq E_{ph} \leq 10.30$ meV. The PC is oscillating with increasing B having a maximum when $\sigma_{xx}(B)$ has a minimum. This is qualitatively similar to our earlier observations.[3] In Fig. 3(b) the photoconductivity for magnetic fields $1.0<B<2.5$ T in the range of laser energies $8.8 \leq E_{laser} \leq 10.30$ meV is shown in a colored plot in comparison to the CR, measured by the transmission of THz waves through the samples in the energy range $8.8 \leq E_{laser} \leq 10.30$ meV. The white line shows the position of the CR in the magnetic field as a function of the radiation energy E_{laser} for $m_c=0.022m_0$. From Fig. 3(b) it is obvious that regions where CR and where bolometric PC can be observed are different. Whereas the bolometric PC is dominant at the SdH minima, the CR shows a linear increase in the position of the CR in the magnetic field as a function of the radiation energy E_{laser}, dominantly at magnetic field values where SdH maxima can be observed. Thus, both the CR and the bolometric PC can be observed in the InSb quantum well samples in separate regions of the magnetic field B. The filling factors for which the bolometric PC is clearly visible correspond to spin gaps at $\nu=5$ and $\nu=7$, and to cyclotron gaps at $\nu=6$ and $\nu=8$. Nevertheless, the PC for different values of E_{ph} behaves qualitatively similar.

In a previous paper we have explained the double-peak structure of $\Delta\sigma_{xx}(B)$ of the nonresonant PR.[4] Due to the heat-

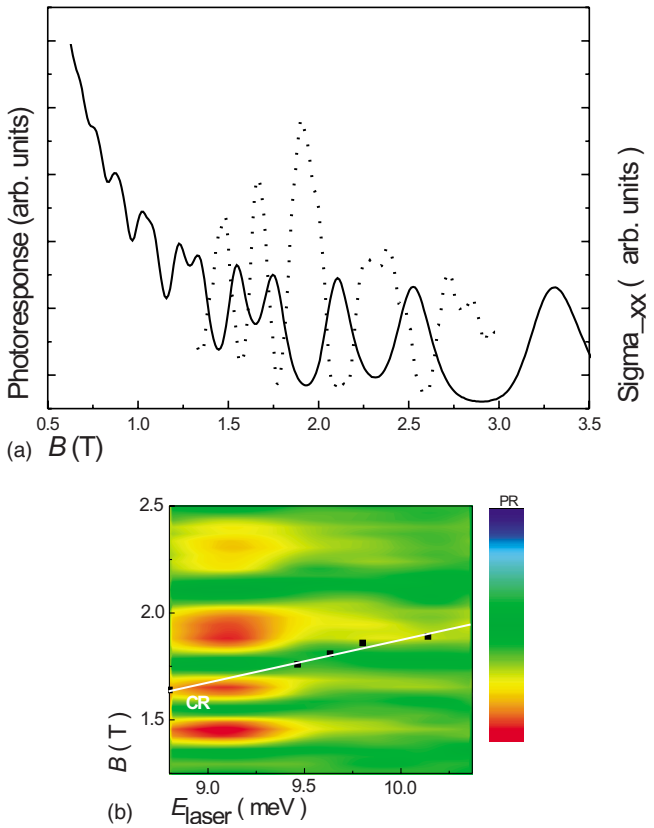

FIG. 3. (Color online) (a) PC (dotted) and the SdH curve $\sigma_{xx}(B)$ for $0.5<B<3.5$ T. (b) Photoconductivity for magnetic fields $1.0<B<2.5$ T in the range of laser energies $8.8\leq E_{laser}\leq 10.30$ meV in a colored plot [red (dark-gray) high PC, green (light gray) low PC] and the measurements of the cyclotron resonance, (CR, black squares, measured by the transmission of THz waves through the samples in the energy range $8.8\leq E_{laser}\leq 10.2$ meV. The white line shows the position of the CR in the magnetic field as a function of the radiation energy E_{laser} for $m_c=0.022m_0$, see the text).

ing of the two-dimensional electron system (2DES) maxima of the nonresonant PR develop at the flanks of the QH plateaus. At higher values of the electrical pre-excitation of the 2DES these two maxima merge and finally become one peak. This development occurs simultaneously with the reduction in width of the QH plateau at higher electrical excitation. The reduction in the magnetic field B (with subsequent increase in the filling factor ν) has a similar effect. As shown in Fig. 3(a), the PR maxima observed at higher ν (for $\nu>6$) possess a singular peak shape. This is due to the reduced cyclotron or spin energy gap at lower B values.

From the transmission measurements, a cyclotron mass according to

$$E_{ph}=\hbar\frac{eB_{res}}{m_c} \tag{1}$$

(B_{res}: magnetic field at which the transmission signal is at its minimum) of $m_c=0.022m_0$ is deduced. This value was confirmed by further transmission measurements at different energies [see the inset in Fig. 2, yielding $m_c=(0.0218\pm 0.0003)m_0$]. This is a value larger than the effective mass at the band edge of InSb, $m^*=0.0139m_0$.[5] The enhancement is due to the nonparabolicity of the band structure of InSb. The effective mass of the first subband level is already slightly enhanced due to its elevated energy value with respect to the band edge. Taking the conduction-band energy profile and the corresponding calculated wave function (see Fig. 4), we can estimate that most of the electrons belonging to the lowest subband possess an energy of 18 meV elevated above the edge of the conduction band. In a two-band approach describing the nonparabolicity of the band structure of InSb,

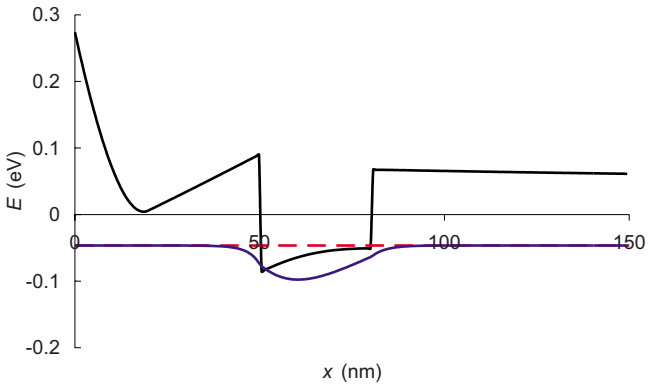

FIG. 4. (Color online) Spatial band scheme and the scheme of the corresponding wave function for the AlInSb/InSb/AlInSb quantum well structure used in this study.

$$m(E)=m^*\left(1+\frac{\alpha E}{E_g}\right) \tag{2}$$

($\alpha=2$ for a two-band approximation derived from the Kane model[6] for the nonparabolic band structure of InSb: E_g is the band-gap energy of 240 meV at low temperatures in InSb), we obtain an effective mass of $m(E=18\ \text{meV})=0.0159m_0$ at the energy of the ground-state subband. Using this value and Eq. (2), we obtain a Fermi energy $E_F=45$ meV above this subband energy from $m_c=0.022m_0$ (see Fig. 2). This position of the Fermi energy can be compared to the value obtained from the electron density deduced from a SdH measurement. Assuming an energy dependence of the mass according to Eq. (2), the relation between the electron density n_s and the Fermi energy E_F is

$$n_s=\int_0^{E_F}D(E)dE=\frac{1}{\pi\hbar^2}\int_0^{E_F}m(E)dE \tag{3}$$

(D: density of states, energy of the ground subband is set to zero). With Eq. (3) and $n_s=2.8\times 10^{15}$ m^{-2} as determined from the period of the SdH oscillation we get $E_F=34$ meV. This is in a reasonable agreement with the value obtained from the transmission measurement. The agreement is, in particular, remarkable in view of the simple two-band model approximation used for these calculations. As the Fermi energy E_F has a maximum position of 45 meV above the ground subband, E_F is located below the next subband which lies at 50 meV above the ground subband. This explains our observation of only one oscillation period in the SdH trace

(see Fig. 1). However, it is conceivable that the SdH oscillations of a higher subband are not resolvable if the population of this subband is lower than the one of the ground-state subband. This is particularly true for the case where the oscillations of a higher subband are visible at lower magnetic fields than those belonging to the ground-state subband. If we apply the value of $\alpha=1.16$ in Eq. (2) (see Ref. 7), we obtain a different set of data. First, the effective mass at the band edge of the ground subband m_{gse} is reduced in that case to a value of $m_{gse}=0.0151m_0$. Accordingly, the difference between the positions of the Fermi energy and the ground subband is $E_F-E_{s0}=85$ meV. Using the value of $\alpha=1.16$, Eq. (3) than yields $E_F-E_{s0}=37$ meV. Thus, our results are better explained with $\alpha=2$. It should be noted here that our experiments differ from those of the study[7] in at least two aspects: first, the pulse energy of our laser is by several orders of magnitude higher than that of the radiation applied in the Fourier-transform spectrometer used in Ref. 7, and second, the energies relevant in Ref. 7 are above 22 meV and around 10 meV in this study. Nevertheless at magnetic fields of $B<2$ T the cyclotron masses presented in Ref. 7 are comparable to the value we measure.

Consequently, the devices made from the wafers with InSb quantum wells are promising for an application as THz detector applications and for the investigation of optically induced spin effects. Further, the basic physical mechanisms of the interaction of THz radiation with the electrons residing in the 2DES of the wafers investigated are of great interest.

IV. SUMMARY

We have investigated the SdH effect, the current-voltage (I_{SD}-V_{SD}) characteristics, the THz transmission, and the THz photoconductivity of various devices patterned on AlInSb/InSb/AlInSb quantum well wafers. From the SdH curves, the electron density and the mobility of the electrons in the quantum well were deduced. At various magnetic fields B corresponding to the SdH minima, the I-V curves showed nonlinearities. Consequently, photoconductivity measurements at appropriate electrical bias values were performed exposing the samples to THz pulses from a p-Ge laser. For samples with contacts produced at a sufficiently high annealing temperature, an oscillating photoconductivity with maximum values at magnetic fields where the conductivity (measured in the dark) shows minimum values is observed. Photoconductivity signals are observable for even and for odd filling factors. These results are interesting for understanding the basic physics of the interaction of a 2DES and THz radiation and for the application of InSb-based devices as THz detectors.

The radiation of the Ge laser was also used for transmission investigations. At a filling factor of $\nu=6$ the cyclotron resonance was clearly observable. The cyclotron mass obtained from these measurements is in agreement with the value to be expected from the electron density deduced from SdH data in a two-band approach deduced from the Kane model for the nonparabolic band structure of InSb.

ACKNOWLEDGMENTS

M. Bugár acknowledges the receipt of a stipend from the Braunschweig International School of Metrology. Yu. B. Vasilyev is partly supported by the Russian Foundation of Basic Research. We acknowledge the use of self-consistent Schrödinger-Poisson code by M. Fearn for Fig. 4.

[1] Yu. L. Ivanov and Yu. B. Vasilyev, Sov. Tech. Phys. Lett. **9**, 264 (1983).
[2] V. N. Shastin, Opt. Quantum Electron. **23**, S111 (1991) , special issue on FIR semiconductor lasers, edited by E. Gornik and A. A. Andronov.
[3] C. Stellmach, G. Vasile, A. Hirsch, R. Bonk, Yu. B. Vasilyev, G. Hein, C. R. Becker, and G. Nachtwei, Phys. Rev. B **76**, 035341 (2007).
[4] G. Nachtwei, F. Gouider, C. Stellmach, G. Vasile, Yu. B. Vasilyev, G. Hein, and R. R. Gerhardts, Phys. Rev. B **78**, 174305 (2008).
[5] E. H. Johnson and D. H. Dickey, Phys. Rev. B **1**, 2676 (1970).
[6] E. O. Kane, J. Phys. Chem. Solids **1**, 249 (1957).
[7] J. M. S. Orr, K.-C. Chuang, R. J. Nicholas, L. Buckle, M. T. Emeny, and P. D. Buckle, Phys. Rev. B **79**, 235302 (2009).